Supplemental Data

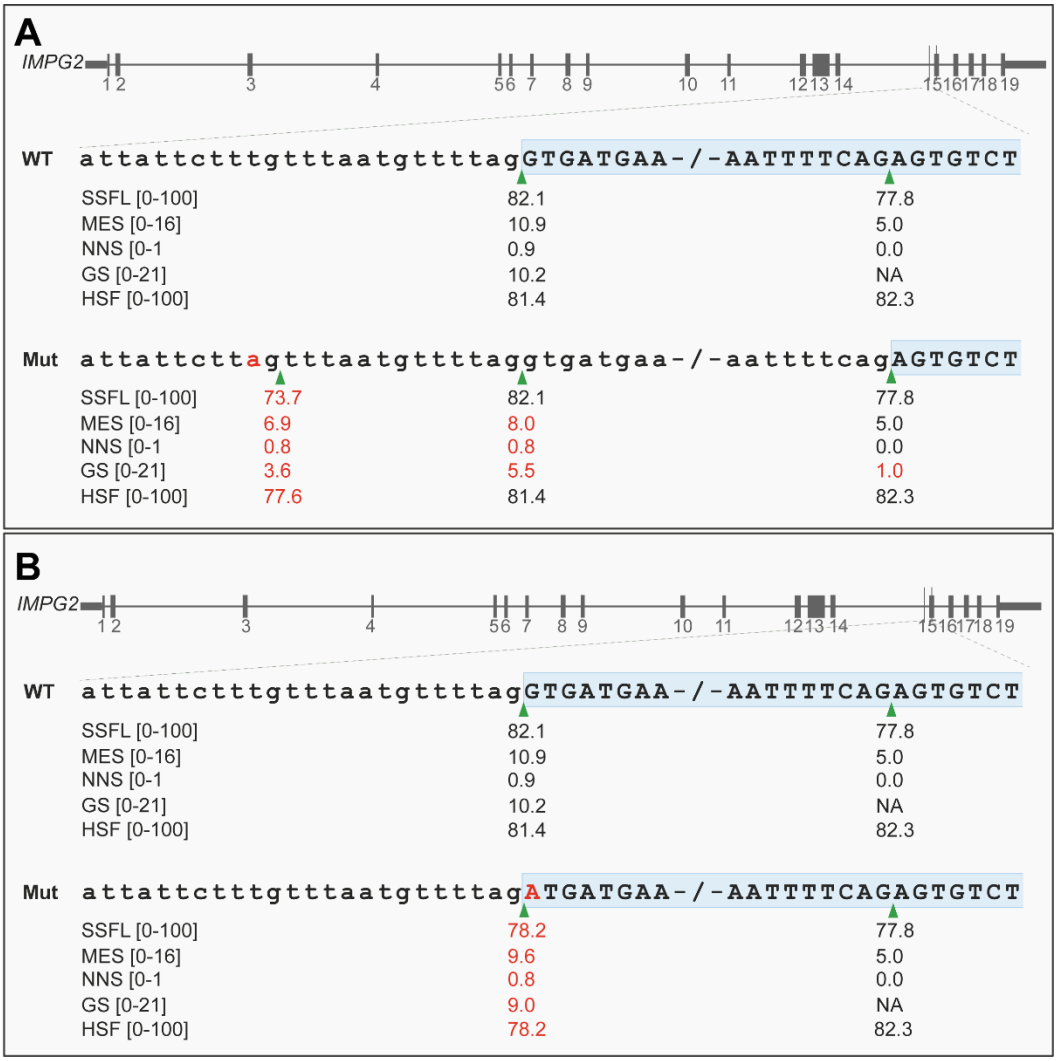

Figure S1: *In silico* splice site predictions for c.3023-15T>A and c.3023G>A. A, B) Schematic representation of *IMPG2* and enlargement of the exon-intron boundary of exon 15 sequence for the wild-type sequence and c.3023-15T>A (A) and c.3023G>A (B). Five *in silico* prediction scores for the splice acceptor site are indicated below each sequence. The green triangles indicate the position of splice acceptor site in both wild-type and mutant sequences. The two red "a" nucleotides highlight the c.3023-15T>A (A) and c.3023G>A (B) variants in the mutant sequence. The red numbers represent the altered scores compared to the wild-type. SSFL, SpliceSiteFinder-Like; MES, MaxEntScan; NNS, NNSPLICE; GS, GeneSplicer; HSF, Human Splice Finder; WT, wild-type; Mut, mutant; NA, not applicable.

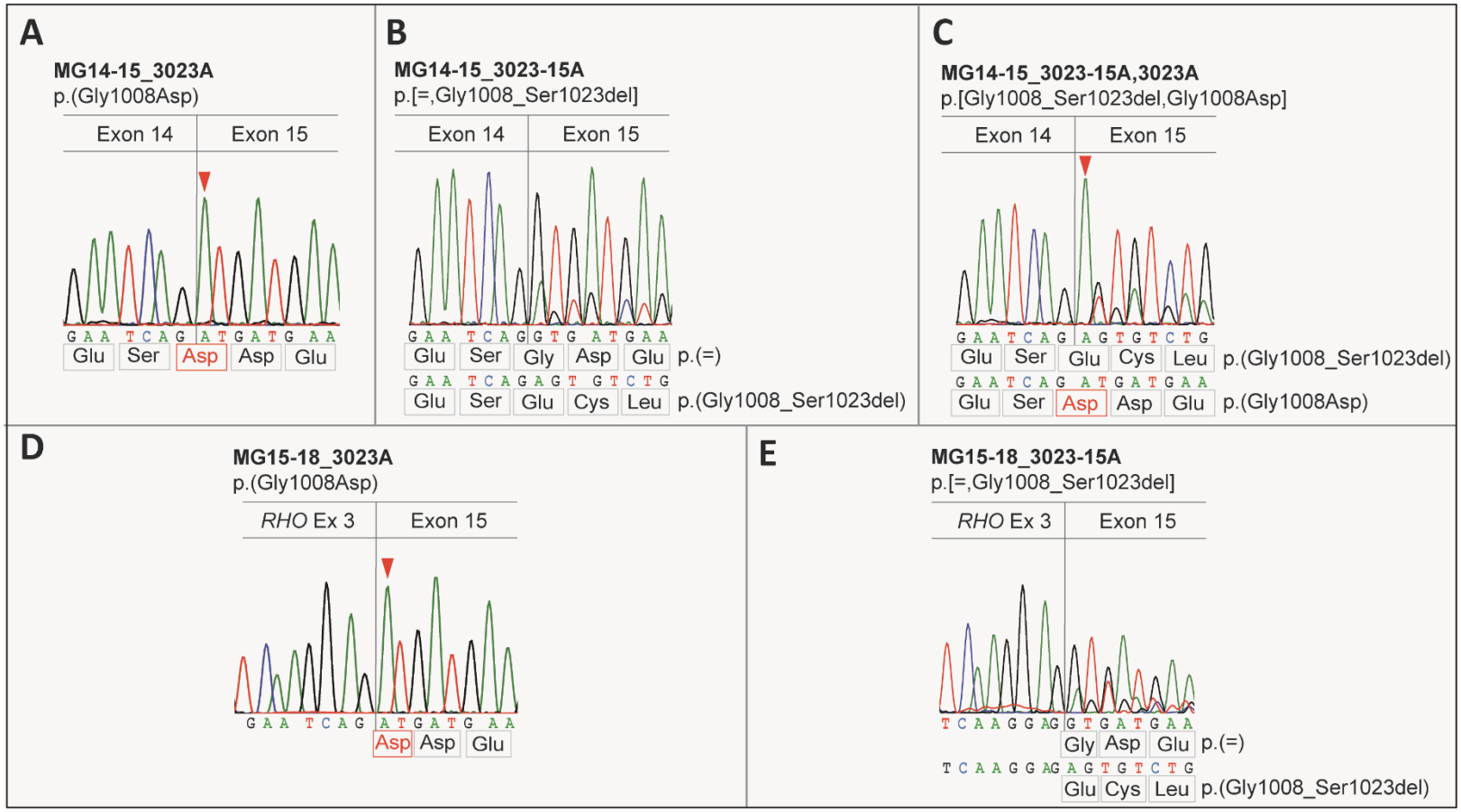

Figure S2: Sanger sequencing chromatograms of RT-PCR products upon transfection of three mutant midigenes in MG14-15, MG15-18_3023-15A, and MG15-18_3023A. A-C) Sequencing chromatograms of RT-PCR products after transfection of three mutated MG14-15 midigenes showed the single nucleotide substitution in c.3023G>A (A), or the combined fragments of the wild-type (upper sequence) and 48-nt deletion (lower sequence) in the presence of c.3023-15T>A variant (B), or the combined fragments of the 48-nt deletion fragment (upper sequence) and the missense fragment (lower sequence). **D-E)** Sequencing chromatograms of RNA products for constructs MG15-18_3023A (D) and MG15-18_3023-15A (E) are shown. The nucleotide substitution in c.3023G>A (D) and the 48-nt deletion fragment together with the large amount of wild-type fragment in c.3023-15T>A were seen (E). The encoded amino acids are depicted for each chromatogram. The Aspartic acid, indicated in red, represents the missense variant (p.(Gly1008Asp)). The red triangle represents the position of variant c.3023G>A.

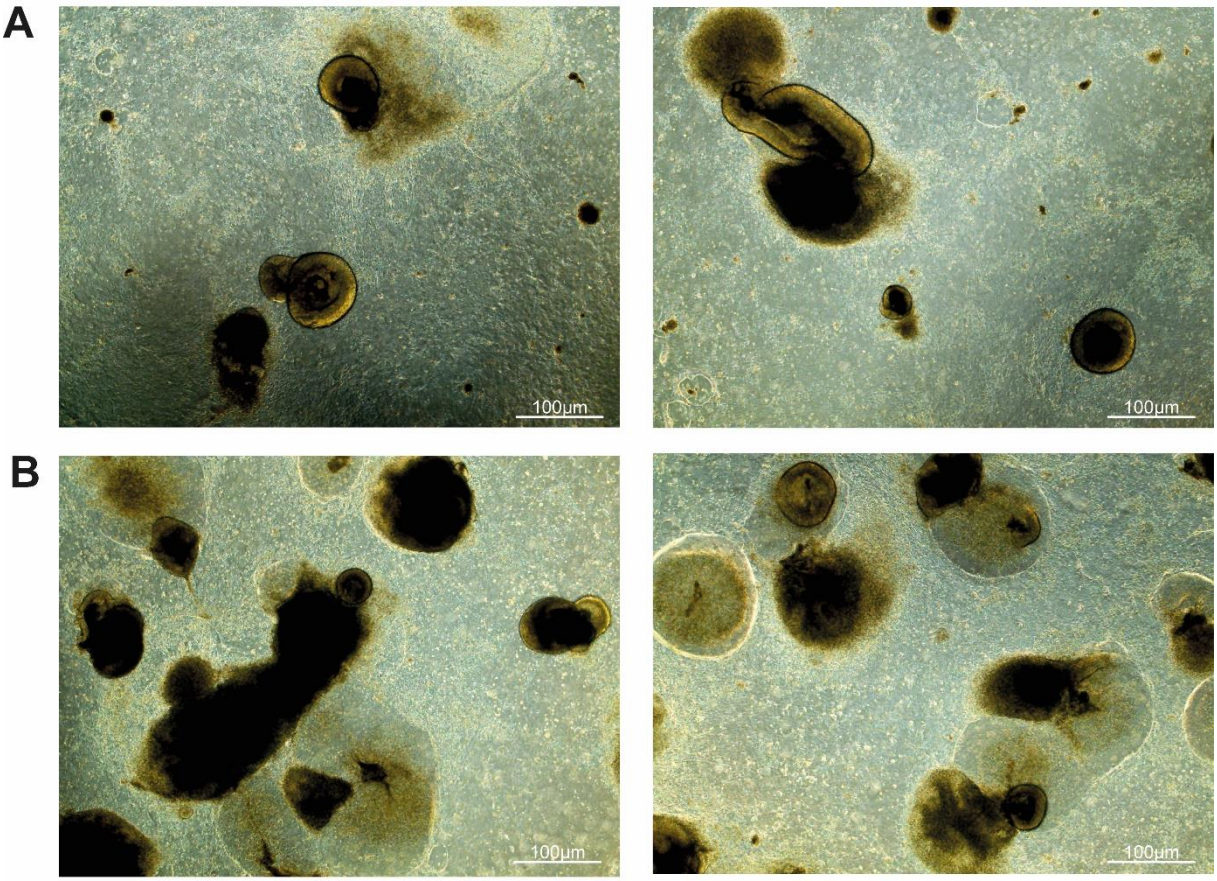

Figure S3. Microscopy images of the photoreceptor precursor cells (PPCs). Representative microscopy images of the PPCs derived from control (A) or patient (B) at day 30 of differentiation. Scale bar represents 100 µm.

Figure S4. Chromatograms of the different splicing events detected using the MG15-18 constructs. Sanger sequencing analysis of the RT-PCR fragments of MG15-18 confirmed the exon 16 deletion in the wild-type, c.3023A, and c.3023-15A constructs of MG15-18 as well as exons 16/17 deletion in the wild-type and c.3023A constructs. The 48-nt deletion of exon 15 in the c.3023-15A and c.3023-15A;3023A constructs was also confirmed. The 48-nt deletion of the exon 15 together with the skipping of the exon 16 or the skipping of exons 16/17 was also confirmed in the c.3023-15A and c.3023-15A;3023A constructs.

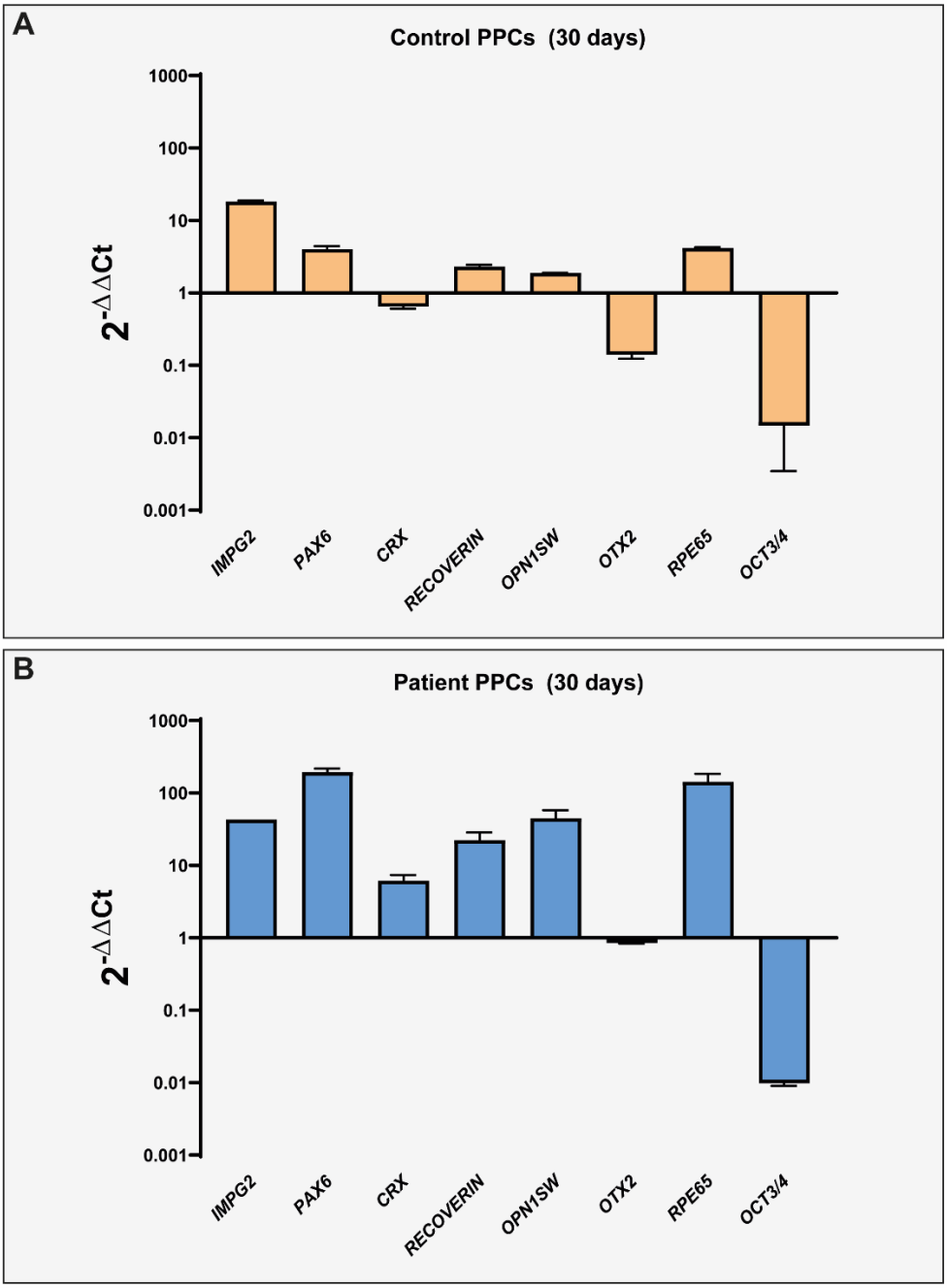

Figure S5. Retinal gene expression profiles of the control and patient-derived photoreceptor progenitor cells (PPCs). Gene expression profile of **A)** control-derived and **B)** patient-derived PPCs from patient B:II-1 after 30 days of differentiation compared to iPSCs (day 0 of differentiation). The differentiation into PPCs is observed by the reduced expression of the pluripotent marker *OCT3/4* and an increased expression of photoreceptor markers. In addition, control and patient B:II-1 PPCs presented an increased expression of *IMPG2*.

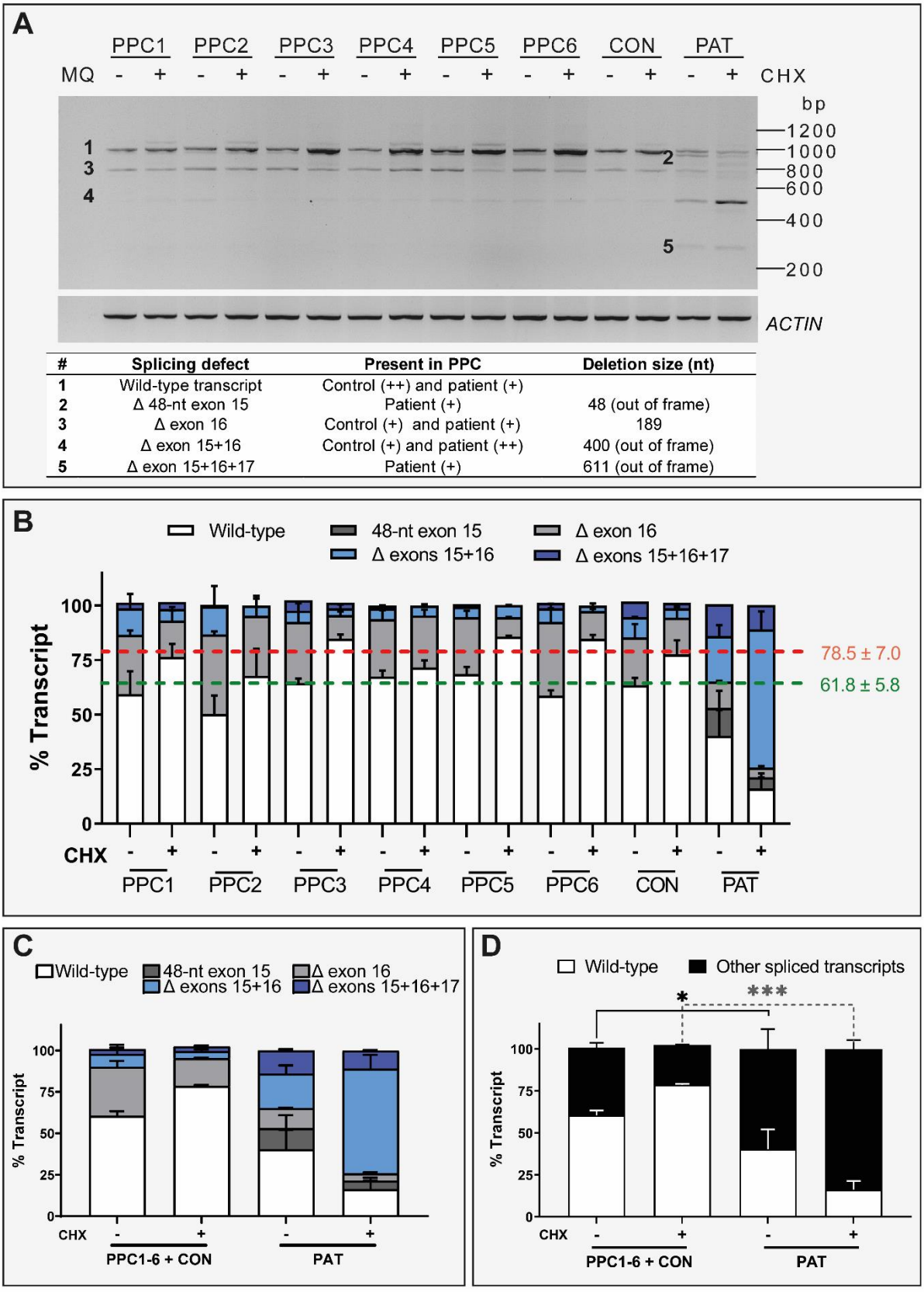

#	Splicing defect	Present in PPC	Deletion size (nt)
1	Wild-type transcript	Control (++) and patient (+)	
2	Δ 48-nt exon 15	Patient (+)	48 (out of frame)
3	Δ exon 16	Control (+) and patient (+)	189
4	Δ exon 15+16	Control (+) and patient (++)	400 (out of frame)
5	Δ exon 15+16+17	Patient (+)	611 (out of frame)

Figure S6. Comparison of the exon 14 to 18 of *IMPG2* splicing readout in different photoreceptor precursor cell (PPC) lines. A) A representative RT-PCR gel picture. Below, the table legend of the transcripts detected on the gel. (+) indicates weak expression and (++) indicates high expression. **B)** The bar chart represents the semi-

quantification of the percentage of each transcript as mean ± SD. The PPC lines were evaluated with cycloheximide treatment (CHX+) and without cycloheximide treatment (CHX-). The dark green line represents the mean of the wild-type transcript expression in the CHX- PPCs, excluding PAT PPCs for the estimation, while the red line represents the wild-type transcript expression of the CHX+ PPCs, also excluding PAT PPCs. **C)** Average of each transcript expression between PPC cell lines (PPC1-7 and CON PPCs) *versus* PAT PPCs. **D)** Graphical representation of the percentage of wild-type and other spliced transcript over the total RNA between PPC cell lines (PPC1-7 + CON PPCs) *versus* PAT-PPCs. For statistical analysis, CHX- conditions or CHX+ conditions were compared. The experiments were performed in duplicate. Statistical significance is indicated as * $p < 0.05$ and *** $p < 0.001$ using one-way ANOVA test. CON: Control-derived PPCs, CHX: cycloheximide, MG14-15: midigene spanning exon 14 and 15, PAT: Patient-derived PPCs, PPC1-7 are non-*IMPG2*-associated PPCs. bp, base pair.

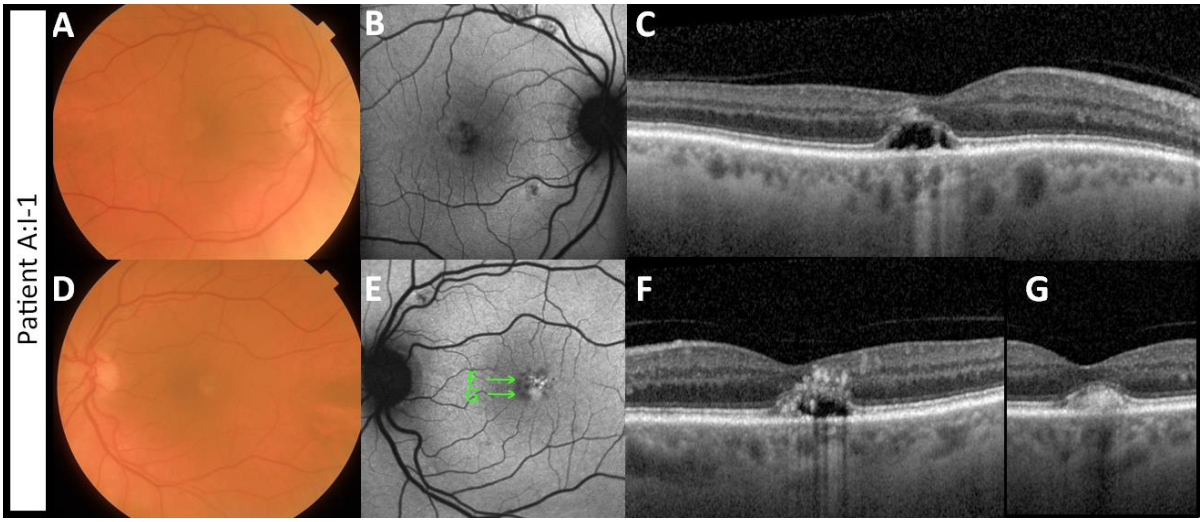

Figure S7. Multimodal imaging of the father of patient A:II-1, carrying the complex allele c.[3023G>A;3023-15T>A]. A-G) Imaging of the right **(A-C**) and left eye (**D-G**) of patient A:I-1 is shown. **A, D)** Fundus photography shows bilateral yellowish vitelliform lesions. **B, E)** Fundus autofluorescence images show a central circular lesion with hypo-and hyperautofluorescent spots. The 'F' and 'G' in green in image E depict the location of the lesion shown in image F and G. **C, F, G)** These correspond to the dome-shaped neuro-epithelium detachment with RPE atrophy. The remaining vitelliform material in the left eye has shifted inferiorly due to gravity. **F, G)** The superior and inferior sectional view of the vitelliform lesion are shown, respectively. Material has also migrated to the inner foveal layer.

A

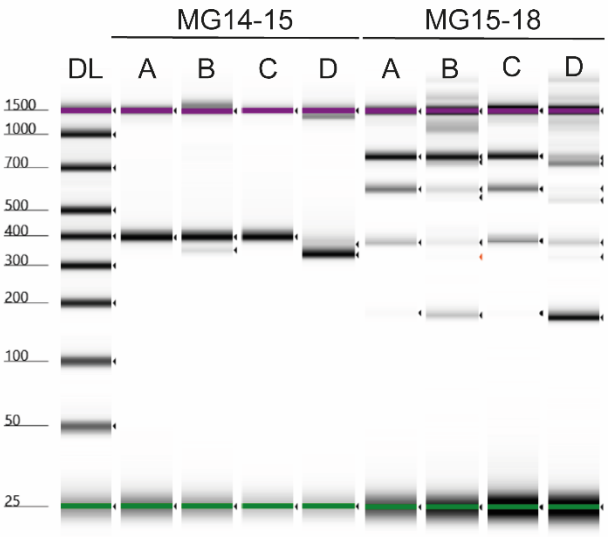

DL: Digital Ladder
A: WT
B: c.3023-15T>A
C: c.3023G>A
D: c.[3023-15T>A;3023G>A]

		% Transcript							
MG14-15		Wild-type		c.3023-15T>A		c.3023G>A		c.[3023-15T>A;3023G>A]	
bp size	Transcript	TS	Fiji	TS	Fiji	TS	Fiji	TS	Fiji
391	Wild-type	100.0	100.0	90.8	95.1	100.0	100.0	18.3	22.7
343	48-nt exon 15	-	-	9.2	4.9	-	-	81.7	77.3

MG15-18		Wild-type		c.3023-15T>A		c.3023G>A		c.[3023-15T>A;3023G>A]	
bp size	Transcript	TS	Fiji	TS	Fiji	TS	Fiji	TS	Fiji
778	Wild-type	52.9	54.3	57.3	65.3	50.2	46.5	11.5	14.8
730	48-nt exon 15	0.0	0.0	9.7	9.6	0.0	0.0	21.8	21.3
589	Δ exon 16	30.1	26.1	9.1	7.9	28.6	30.3	1.7	2.1
541	Δ exon 16 - 48-nt exon 15	-	-	1.4	-	-	-	4.6	2.1
378	Δ exons 16+17	15.8	19.6	3.2	4.7	20.7	23.2	9.2	9.7
330	Δ exons 16+17 + 48-nt exon 15	0.0	0.0	3.2	1.0	0.0	0.0	1.6	2.4
169	Δ exons 16+17+18	1.3	0.0	16.1	11.6	0.6	0.0	49.6	47.6

B

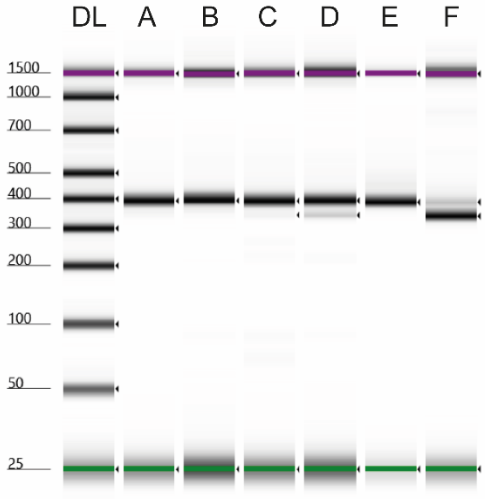

DL: Digital Ladder
A: CON PPC CHX-
B: CON PPC CHX+
C: PAT PPC CHX-
D: PAT PPC CHX+
E: MG14-15 WT
F: MG14-15 c.[3023-15T>A;3023G>A]

		% Transcript											
		CON PPC				PAT PPC				MG14-15			
exon 14 to exon 15		CHX-		CHX+		CHX-		CHX+		Wild-type		c.[3023-15T>A;3023G>A]	
bp size	Transcript	TS	Fiji	TS	Fiji	TS	Fiji	TS	Fiji	TS	Fiji	TS	Fiji
391	Wild-type	100.0	99.6	100.0	99.3	93.6	95.0	88.3	93.4	100.0	100.0	19.7	38.5
343	Δ 48-nt exon 15	-	0.4	-	0.7	6.4	5.0	11.7	6.6	-	-	80.4	61.5

Figure S8. Semiquantitative comparison of *IMPG2* transcripts using TapeStation system and Fiji software in midigenes. A) The upper panel shows a representative digital gel obtained after the TS analysis of the MG14-15 and MG15-18 constructs (n=2). The lower panel shows the average percentage value of each detected transcript by TS analysis (n=2) or Fiji (n=3) for the different variants integrated in the MG14-15 and MG15-18 . **B)** The upper

panel shows a representative digital gel obtained after the TS analysis of the control (CON) and patient (PAT) derived photoreceptor precursor cells (PPCs) as well as two of the relevant MG14-15 constructs (WT and c.[3023-15T>A;3023G>A]). The PPC lines were evaluated with cycloheximide treatment (CHX+) and without cycloheximide treatment (CHX-). The lower panel indicates the average percentage of each detected transcript between TS (n=2) and Fiji (n=2). bp: base pairs; TS: TapeStation.

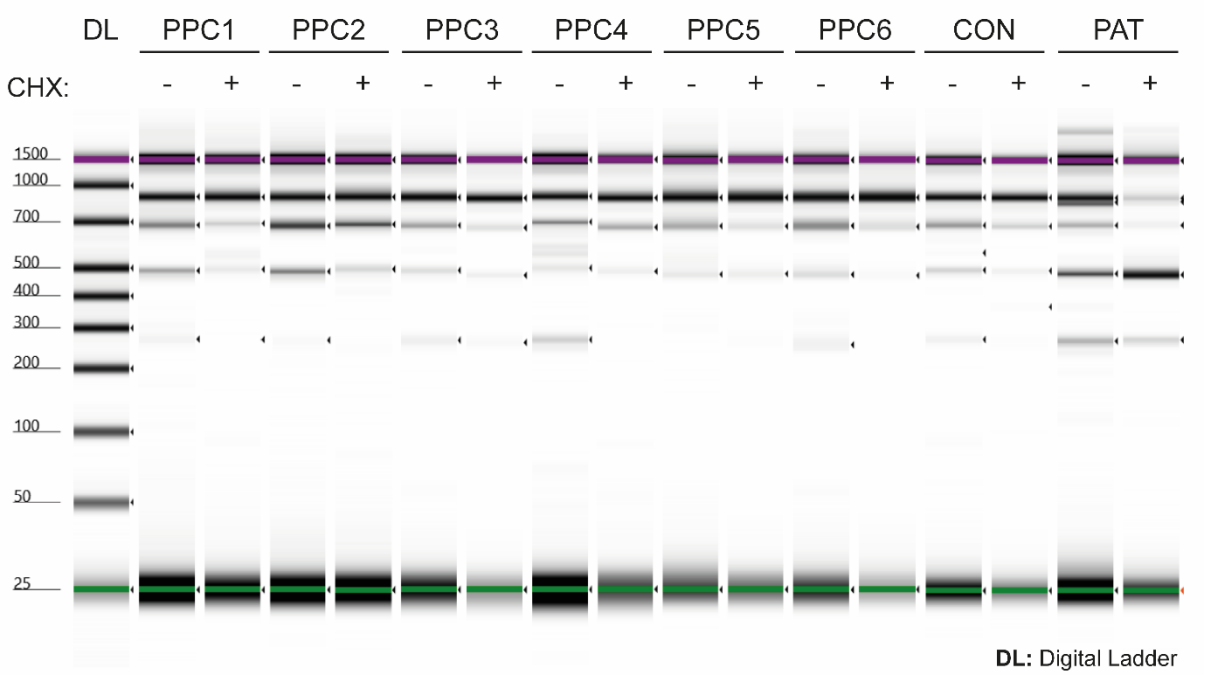

		% Transcript															
		PPC1				PPC2				PPC3				PPC4			
PPCs: 1 to 4		CHX-		CHX+		CHX-		CHX+		CHX-		CHX+		CHX-		CHX+	
bp size	Transcript	TS	FIJI	TS	FIJI	TS	FIJI	TS	FIJI	TS	FIJI	TS	FIJI	TS	FIJI	TS	FIJI
918	Wild-type	59.4	78.1	76.5	81.4	50.3	64.7	67.8	73.4	64.5	67.0	84.8	83.5	67.5	69.5	71.6	75.5
870	Δ 48-nt exon 15	-	-	-	-	-	-	-	-	-	-	-	-	-	-	-	-
700	Δ exon 16	27.1	21.3	16.6	17.1	36.5	30.2	27.5	21.0	27.9	32.3	10.8	11.2	26.3	27.5	23.8	23.0
500	Δ exons 15+16	12.1	0.7	5.3	1.4	12.9	5.1	4.7	0.6	5.1	0.4	3.1	3.9	4.9	3.0	4.6	1.2
270	Δ exons 15+16+17	1.3	-	1.6	-	0.4	-	-	5.0	2.4	0.3	1.3	1.3	1.3	-	-	0.3
		PPC5				PPC6				CON				AVERAGE			
PPCs: 5 and 6; CON PPC		CHX-		CHX+		CHX-		CHX+		CHX-		CHX+		CHX-		CHX+	
bp size	Transcript	TS	FIJI	TS	FIJI	TS	FIJI	TS	FIJI	TS	FIJI	TS	FIJI	TS	FIJI	TS	FIJI
918	Wild-type	68.5	70.1	85.8	86.3	58.7	70.3	84.7	82.9	63.5	73.2	77.6	81.4	61.8	70.4	78.4	80.6
870	Δ 48-nt exon 15	-	-	-	-	-	-	-	-	-	-	-	-	-	-	-	-
700	Δ exon 16	26.2	26.4	8.9	7.8	33.7	24.2	12.7	13.2	21.9	20.5	16.9	15.3	28.5	26.0	16.7	15.5
500	Δ exons 15+16	4.8	2.9	5.5	5.8	6.3	5.5	2.6	3.9	9.2	5.1	4.3	3.3	7.9	3.2	4.3	2.9
270	Δ exons 15+16+17	0.6	0.6	-	-	1.3	-	-	-	5.4	1.3	1.3	-	1.8	0.3	0.6	0.9

		% Transcript			
		PAT			
PAT		CHX-		CHX+	
bp size	Transcript	TS	FIJI	TS	FIJI
918	Wild-type	40.3	41.0	16.2	25.5
870	Δ 48-nt exon 15	12.7	14.5	5.2	5.2
700	Δ exon 16	12.1	7.9	4.4	1.8
500	Δ exons 15+16	20.8	20.7	63.3	52.8
270	Δ exons 15+16+17	14.0	16.0	10.8	14.7

Figure S9. Comparison of the TapeStation system and Fiji software for estimating transcript percentages in photoreceptor precursor cells (PPCs). The upper panel depicts a representative digital gel obtained after the TS analysis different PPCs derived from non-*IMPG2*-associated IRD individuals (PPC1-6), the control-derived PPCs (CON) and the patient-derived PPCs (PAT) (n=2). All PPC lines were evaluated with cycloheximide treatment (CHX+) and without cycloheximide treatment (CHX-). The lower panel shows the average percentage of each detected transcript per PPC line discerning between TS (n=2) and Fiji (n=2) estimations. The average values of the non-*IMPG2*-associated IRD and control derived PPCs are highlighted in gray. bp: base pairs; TS: TapeStation.

Table S1: Details of primers designed for MG14-15 and MG15-18 midigene splice constructs

Name	Sequence (5' to 3')	Tm (°C)	GC%	Size (nt)
***IMPG2*_Ex14-Ex15_tag_F**	GATAAAATACAATTAGGAAAAGTGAGG	57.2	29.6	10,390
***IMPG2*_Ex14-Ex15_tag_R**	GATGGCTCCCATCTATTGC	58.1	52.6	
***IMPG2*_Ex15-Ex18_tag_F**	TGGAAATGAATGGTCCATGA	59.7	40.0	4,847
***IMPG2*_Ex15-Ex18_tag_R**	TCTGCCACTGGCTATCACTG	60.0	55.0	
***IMPG2*_Exon 15_ F**	TGCACAAAAATTTGACAAAAGC	60.1	31.8	367
***IMPG2*_Exon 15_ R**	TTCAAGCAGAAGTCAGGCTGT	60.1	47.6	
Mut_*IMPG2*_c.3023-15T>A_F	GCTTCATCACCTAAAACATTAAACTAAGAATAATGCAAGAAAAGGCAAA	76.6	30.6	12,649 (MG14-15) 9,547 (MG15-18)
Mut_*IMPG2*_c.3023-15T>A_R	TTTGCCTTTTCTTGCATTATTCTTAGTTTAATGTTTTAGGTGATGAAGC	76.6	30.6	
Mut_*IMPG2*_c.3023G>A_F	TGCAAGGGTTGGCTTCATCATCTAAAACATTAAACAAAGAATAATGC	79.1	34.0	12,649 (MG14-15) 9,547 (MG15-18)
Mut_*IMPG2*_c.3023G>A_R	GCATTATTCTTTGTTTAATGTTTTAGATGATGAAGCCAACCCTTGCA	79.1	34.0	
Mut_*IMPG2*_NCSS.mis_F	GCTTCATCATCTAAAACATTAAACTAAGAATAATGCAAGAAAAGGCAAA	75.8	28.6	12,649 (MG14-15) 9,547 (MG15-18)
Mut_*IMPG2*_NCSS.mis_R	TTTGCCTTTTCTTGCATTATTCTTAGTTTAATGTTTTAGATGATGAAGC	75.8	28.6	
Mut_IMPG2_c.[3069A>C;3072G>A]_F	GCAAGTTTCAGGCCTGTAATGAATTTTCCGAATGTCTGGTCAACCCCTGGAGTGG	84.1	49.1	12,649 (MG14-15) 9,547 (MG15-18)
Mut_*IMPG2*_c.[3069A>C;3072G>A]_R	CCACTCCAGGGGTTGACCAGACATTCGGAAAATTCATTACAGGCCTGAAACTTGC	84.1	49.1	
***IMPG2*_RT-PCR_Exon 14_F**	CACGGGGTTCCAGAACTTAG	59.5	55.0	391
***IMPG2*_RT-PCR_Exon 15_R**	GTGCCCAGGCATAATGTCAC	61.3	55.0	
***RHO*_Exon 3_F**	CGGAGGTCAACAACGAGTCT	64.7	55.0	778
***IMPG2*_RT-PCR_Exon 18_R**	TGCAAACTCAGGATCATTGG	59.6	45.0	
***RHO*_Exon 5_F**	ATCTGCTGCGGCAAGAAC	64.7	55.6	140
***RHO*_Exon 5_R**	AGGTGTAGGGGATGGGAGAC	64.5	60.0	

Sequence of all designed primers midigene assay with GC content and melting temperature, tm(°C) and size of PCR products (Ex, exon; midigene exon14-15; MG15-18, midigene exon15-18).

Table S2. qPCR primers list. All qPCR were conducted using an annealing temperature of 60°C.

Name	Sequence (5' to 3')	GC%	Fragment size (nt)
***PAX6*_qPCR_F**	GCTGCAAAGAAATAGAACATCC	41.0	111
***PAX6*_qPCR_R**	TTGGCTGCTAGTCTTTCTCG	50.0	
***CRX*_qPCR_F**	CCCCAGTGTGGATCTGATG	58.0	116
***CRX*_qPCR_R**	CAAACAGTGCCTCCAGCTC	58.0	
***RECOVERIN*_qPCR_F**	ACACCAAGTTCTCGGAGGAG	55.0	108
***RECOVERIN*_qPCR_R**	ACTTGGCGTAGATGCTCTGG	55.0	
***OPN1SW*_qPCR_F**	TTCTTCTCCAAGAGTGCTTGC	48.0	97
***OPN1SW*_qPCR_R**	CCTTCCCACACACCATCTTC	55.0	
***OTX2*_qPCR_F**	TATCTTAAGCAACCGCCTTACG	45.0	75
***OTX2*_qPCR_R**	GGAGGGGTGCAGCAAGTC	67.0	
***RPE65*_qPCR_F**	TTACTACGCTTGCACAGAGACC	50.0	105
***RPE65*_qPCR_R**	GCCCCATTGACAGAGACATAG	52.0	
***OCT3/4*_qPCR_F**	GTTCTTCATTCACTAAGGAAGG	41.0	101
***OCT3/4*_qPCR_R**	CAAGAGCATCATTGAACTTCAC	41.0	
***GUSB*_qPCR_F**	AGAGTGGTGCTGAGGATTGG	55.0	80
***GUSB*_QPCR_R**	CCCTCATGCTCTAGCGTGTC	60.0	
***IMPG2*_qPCR_F**	GCTTAATCATGAAGAAACTGAC	33.0	107
***IMPG2*_qPCR_R**	GAGAGTAGTGTCTCCCAATG	50.0	

Table S3. Primer set employed in the splicing analysis in photoreceptor precursor cells (PPCs).

Name	Sequence (5' to 3')	Tm (°C)	GC%	Size (nt)
***IMPG2*_RT-PCR_Exon 14_F**	CACGGGGTTCCAGAACTTAG	59.5	55.0	391
***IMPG2*_RT-PCR_Exon 15_F**	CGGAGGTCAACAACGAGTCT	64.7	55.0	
***IMPG2*_RT-PCR_Exon 14_F**	CACGGGGTTCCAGAACTTAG	59.5	55.0	861
***IMPG2*_RT-PCR_Exon 18_R**	TGCAAACTCAGGATCATTGG	59.6	45.0	
***ACTIN*_exon3_F**	ACTGGGACGACATGGAGAAG	60.5	55.0	398
***ACTIN*_exon4_R**	TCTCAGCTGTGGTGGTGAAG	60.5	55.0	

Table S4: Individual and complex allele *IMPG2* variant in silico prediction scores.

DNA variant	Splice site position	SSFL [0-100]			Max EntScan [1-16]			NN SPLICE [0-1]			Gene Splicer [0-21]			HSF [0-100]		
		WT	Mut	Delta %	WT	Mut	Delta %	WT	Mut	Delta %	WT	Mut	Delta %	WT	Mut	Delta %
c.3023-15T>A	c.3023-14	-	73.7	**-73.7**	-	6.9	**-43.1**	-	0.8	**-80.0**	-	3.6	**-17.1**	-	77.6	**-77.6**
	c.3023-1	82.1	82.1	**0.0**	10.9	8.0	**18.1**	0.9	0.8	**10.0**	10.2	5.5	**22.3**	81.4	81.4	**0.0**
c.3023G>A	c.3023-1	82.1	78.2	**3.9**	10.9	9.6	**8.1**	0.9	0.8	**10.0**	10.2	9.0	**10.0**	81.4	78.2	**3.2**
c.[3023-15T>A; 3023G>A]	c.3023-14	-	73.7	**-73.7**	-	6.9	**-43.1**	-	0.9	**-90.0**	-	3.9	**-18.6**	-	77.6	**-77.6**
	c.3023-1	82.1	78.2	**3.9**	10.9	6.7	**26.2**	0.9	0.5	**40.0**	10.2	4.4	**27.6**	81.4	78.2	**3.2**

SSFL, SpliceSiteFinder-Like (0-100); MaxEntScan (0-12 for donor sites_0-16 for acceptor sites); NNSPLICE (0-1); GeneSplicer (0-24 for donor sites_0-21 for acceptor sites); HSF, Human Splicing Finder (0-100); WT, wild-type; Mut, mutant. The "-" indicates an unrecognized splice site.

Table S5: The SpliceAI scores for variants c.3023-15T>A and c.3023G>A in *IMPG2*.

DNA allele	c.3023-15T>A	c.3023G>A
Delta score_ Acceptor gain	0.37	0.25
Delta score_ Acceptor loss	0.47	0.01
Delta score_ Donor gain	0	0
Delta score_ Donor loss	0.12	0.03
Delta position_ Acceptor gain	-2	-48
Delta position _ Acceptor loss	-15	0
Delta position_ Donor gain	-15	-48
Delta position_ Donor loss	-221	-206

The positions are based on the distance from the variant; positive numbers upstream and negative numbers in the downstream direction.

Table S6: The percentage of each fragment in wild-type and mutant midigenes after RT-PCR analysis (calculated using Fiji).

***IMPG2* Construct MG14-15**					
MG14-15_c.3023-15A	**Raw intensity**	**Fragment size (nt)**	**Correction factor**	**Corrected intensity**	**Percentage**
WT	13133.2	391	1	13133.1	100%
Mut_larger fragment	11887.5	391	1	11887.5	95.1%
Mut_smaller fragment	540.4	343	0.87	616.03	4.9%
MG14-15_3023-15A;3023A					
WT	7660.9	391	1	7660	100%
Mut_larger fragment	6322.8	391	1	6322.8	22.7%
Mut_smaller fragment	18591.8	343	0.87	21193.6	77.3%
***IMPG2* Construct MG15-18**					
MG15-18_WT					
WT_ 778-nt fragment	15171.9	778	1	15171.9	73.0%
WT_589-nt fragment	3691.9	589	0.75	4876.6	22.3%
WT_378-nt fragment	493.1	378	0.48	1014.7	4.7%
MG15-18_c.3023-15A					
c.3023-15A_ 778-nt fragment	9128.1	778	1	9128.1	92.2%
c.3023-15A_ 730-nt fragment	237.5	730	0.94	253.2	3.0%
c.3023-15A_ 589-nt fragment	365.1	589	0.76	482.2	4.8%
MG15-18_c.3023A					
c.3023A_ 778-nt fragment	14453.1	778	1	14453.1	73.7%
c.3023A_589-nt fragment	3161.1	589	0.75	4175.3	21.0%
c.3023A_378-nt fragment	535.7	378	0.48	1102.6	5.3%
MG15-18_c.3023-15A;3023A					
c.3023-15A,3023A _ WT fragment	65268.2	778	1	65268.2	65.4%
c.3023-15A,3023A _ Mut fragment	41747.9	730	0.93	44492.9	34.6%

WT, wild-type; Mut, mutant; MG14-15, midigene exon14-15; MG15-18, midigene exon15-18.

Supplemental methods

Variant prioritization

Moreover, a putative splicing defect was evaluated for synonymous, non-coding splice site and near exon aberrant RNA (NEAR) variants as previously described[1] using algorithms including SpliceSiteFinder-like (SSFL)[2], MaxEntScan (MES)[3], NNSPLICE (NNS)[4], GeneSplicer (GS)[5], and Human Splicing Finder (HSF)[6] embedded in the Alamut Visual software version 2.10 (Interactive Biosoftware, Rouen, France; http://www.interactive-biosoftware.com). Additionally, the prioritized putative pathogenic non-coding variants were assessed by the SpliceAI algorithm prior to *in vitro* functional analyses[7]. Modified from the default-setting, we consider the non-coding variants with at least one delta score above the threshold of 0.01 for gain or loss in a splice acceptor site (SAS) or splice donor site (SDS) for assessment in midigene splice assays[8]. Five hundred nt upstream and downstream of a variant were included as input sequences for SpliceAI analysis. The pathogenic variant data is submitted to Leiden Open Variation Database (LOVD).

In Vitro Splice Assays

Each generated wild-type construct (MG14-15_WT and MG15-18_WT) was utilized as a template to generate three mutant constructs including c.3023G>A, c.3023-15T>A, and the complex allele c.[3023-15T>A;3023G>A] by site-directed mutagenesis PCR. Subsequently, all generated constructs (two wild-type and six mutant constructs) were independently incorporated into the pCI-*NEO-RHO* Gateway-adapted vector to generate wild-type and mutant midigenes.

Eight midigenes were separately transfected into HEK293T (Human embryonic kidney 293; ATCC# CRL-3216™) using FuGENE-HD (Promega, WI, USA) following manufacturer's protocols for the ratio 1:3 for minigene transfection. HEK293T cells were cultured in Dulbecco's Modified Eagle Medium (DMEM) supplemented with 10% FBS, 1% sodium pyruvate and 1% penicillin–streptomycin at 37 °C and 5% CO_2. After 48 hours, cells were harvested RNA was isolated (NucleoSpin RNA, Macherey-Nagel, Bethlehem, PA, USA) and retrotranscribed into cDNA (iSCRIPT, Bio-Rad, Hercules, CA, USA) following the manufacturer's protocol. Ultimately, the transcripts were analyzed by reverse transcription–polymerase chain reaction (RT-PCR) with primers in exons 14 and 15 and in *RHO* exon 3 and *IMPG2* exon 18 for the respective construct. All mixtures of PCR reaction (total 25 µl volume) contained 0.2 µM of each primer pair, 1 U Taq DNA Polymerase (Roche, Basel, Switzerland), 1X PCR buffer with $MgCl_2$, 1 mM $MgCl_2$, 0.2 mM dNTPs, 1X Q-Solution (QIAGEN, Hilden, Germany), and 50 ng cDNA. The PCR thermocycler program included a denaturation step of 94°C for 5 min, followed by 35 cycles of melting (94°C for 30 s), annealing (58°C for 30 s), and extension (72°C for 5 min) steps, with a final elongation step of 72°C for 2 min. Finally, the semi-quantification of the different transcripts was performed using Fiji software[9] (Table S6) and by employing a 1:50 dilution of the RT-PCR product in a TapeStation (Agilent, CA, USA). The comparison between both systems is included in Figures S8 and S9.

Induced pluripotent stem cell (iPSC) differentiation into photoreceptor precursor cells (PPCs)

The differentiation into PPCs was performed as described previously[10-12]. Briefly, iPSC cells were seeded as single cells in a 6-well plate previously coated with 1:20 matrigel (Corning, NY, USA). Cells were cultured in Essential 8 Flex medium (Gibco, TX, USA), supplemented with a final concentration 10 µM ROCK inhibitor (Sigma-Aldrich, MO, USA) and 20 µM primocin (ant-pm-2;Invitrogen, MA, USA) until confluent. Once confluent, differentiation was started by replacing the medium by CI medium (DMEM/F-12 (Dulbecco's Modified Eagle Medium: Nutrient Mixture F-12) supplemented with non-essential amino acids (x100; Sigma-Aldrich) N2 supplement (x100; Gibco), B-27 supplement (x100, Gibco), Human recombinant bFGF (10 ng/µl; Stemcell technologies, Vancouver, Canada), heparin sodium (10 µg/µl; Sigma-Aldrich), Insulin-like Growth Factor-I human (100 ng/µl; Sigma-Aldrich), Recombinant Human COCO Protein (200 µg/ml; Sigma-Aldrich) and 20 µM primocin. Half of the medium was replaced on a daily basis for 30 days.

Semi-quantification by Fiji software and TapeStation analysis

To adequately semi-quantify large and smaller sized fragments we applied both the Fiji semi-quantification[13] as well as the TapeStation method. For TapeStation, the RT-PCR products were measured in DeNovix DS-11 Series

Spectrophotometer (DeNovix, DE, USA) by making a dilution to get a final concentration between 100-500 pg in all the samples. Then, High-Sensitivity D1000 kit (Agilent, CA, USA) was employed to assess the percentage of each transcript following the manufacturer's instructions. The percentage of each transcript was calculated by comparing to the sum of all bands. This calculation was performed by the software directly taking into account the size of the product. For Fiji semi-quantification, we used the rectangle tool, followed by the intensity area calculation. Subsequently each lane was considered 100% and the percentage of each transcript was calculated. As larger fragments retained more ethidium bromide and therefore are more intense, we corrected by fragment size (table S6).

References

1. Fadaie Z, Khan M, Del Pozo-Valero M, et al. Identification of splice defects due to noncanonical splice site or deep-intronic variants in ABCA4. *Hum Mutat* 2019;40:2365-2376.
2. Shapiro MB, Senapathy P. RNA splice junctions of different classes of eukaryotes: sequence statistics and functional implications in gene expression. *Nucleic acids research* 1987;15:7155-7174.
3. Reese MG, Eeckman FH, Kulp D, Haussler D. Improved splice site detection in Genie. *J Comput Biol* 1997;4:311-323.
4. Yeo G, Burge CB. Maximum entropy modeling of short sequence motifs with applications to RNA splicing signals. *J Comput Biol* 2004;11:377-394.
5. Pertea M, Lin X, Salzberg SL. GeneSplicer: a new computational method for splice site prediction. *Nucleic Acids Res* 2001;29:1185-1190.
6. Desmet FO, Hamroun D, Lalande M, Collod-Béroud G, Claustres M, Béroud C. Human Splicing Finder: an online bioinformatics tool to predict splicing signals. *Nucleic Acids Res* 2009;37:e67.
7. Jaganathan K, Kyriazopoulou Panagiotopoulou S, McRae JF, et al. Predicting Splicing from Primary Sequence with Deep Learning. *Cell* 2019;176:535-548 e524.
8. Khan M, Cornelis SS, Pozo-Valero MD, et al. Resolving the dark matter of ABCA4 for 1054 Stargardt disease probands through integrated genomics and transcriptomics. *Genet Med* 2020;22:1235-1246.
9. Rueden CT, Schindelin J, Hiner MC, et al. ImageJ2: ImageJ for the next generation of scientific image data. *BMC Bioinformatics* 2017;18:529.
10. Albert S, Garanto A, Sangermano R, et al. Identification and Rescue of Splice Defects Caused by Two Neighboring Deep-Intronic ABCA4 Mutations Underlying Stargardt Disease. *Am J Hum Genet* 2018;102:517-527.
11. Garanto A, Duijkers L, Tomkiewicz TZ, Collin RWJ. Antisense Oligonucleotide Screening to Optimize the Rescue of the Splicing Defect Caused by the Recurrent Deep-Intronic ABCA4 Variant c.4539+2001G>A in Stargardt Disease. *Genes (Basel)* 2019;10.
12. Khan M, Arno G, Fakin A, et al. Detailed Phenotyping and Therapeutic Strategies for Intronic ABCA4 Variants in Stargardt Disease. *Mol Ther Nucleic Acids* 2020;21:412-427.
13. Schindelin J, Arganda-Carreras I, Frise E, et al. Fiji: an open-source platform for biological-image analysis. *Nat Methods* 2012;9:676-682.